Angewandte Chemie International Edition

Angewandte International Edition Chemie

How to cite: *Angew. Chem. Int. Ed.* **2026**, e3335355
doi.org/10.1002/anie.3335355

COMMUNICATION

Achieving 1.0-s Thermally Activated Delayed Fluorescence via Synergistic Control of Reverse Intersystem Crossing and Exciton Cycling

Yue Lei[1] | Ruyi Liu[1] | Yuling He[1] | Guiyin Luo[1] | Chuanhao Liu[2] | Jiaqi Su[1] | Binhao Li[1] | Xue Long[1] | Yuchang Tan[1] | Yanju Luo[2] | Hailin Qiu[3] | Yan Huang[1] | Zhiyun Lu[1]

[1]Key Laboratory of Green Chemistry and Technology (Ministry of Education), College of Chemistry, Sichuan University, Chengdu, China | [2]Analytical & Testing Center, Sichuan University, Chengdu, China | [3]Orient KOJI Limited, Tianjin, China

Correspondence: Yan Huang (huangyan@scu.edu.cn) | Zhiyun Lu (luzhiyun@scu.edu.cn)

Received: 22 February 2026 | **Revised:** 2 May 2026 | **Accepted:** 4 June 2026

Keywords: exciton cycling | lifetime prolongation | persistent thermally activated delayed fluorescence | reverse intersystem crossing | synergistic control

ABSTRACT

Persistent thermally activated delayed fluorescence (p-TADF) is fundamentally constrained by the kinetic trade-off between reverse intersystem crossing (rISC) and triplet exciton decay, including phosphorescence and non-radiative processes, which intrinsically limits its lifetime (τ_{DF}). Here we present a synergistic strategy that overcomes this limitation by concurrently slowing the rISC rate (k_{rISC}) while preserving the condition $k_{rISC} \gg k_{Ph} + k_{nr,T}$ and deliberately promoting multiple intersystem crossing (ISC)/rISC exciton cycles. The efficacy of this approach is validated by *o*-TFBCz, which achieves an unprecedented τ_{DF} of 1.00 s even in unannealed poly(methyl methacrylate), despite originating from a phosphorescence core with a lifetime (τ_{Ph}) of only 1.92 s. This system exhibits bluish-green afterglow under blue-light excitation and outstanding thermal stability. Quantitative photophysical analysis reveals an average of 2.1 ISC/rISC cycles per exciton in this material, enabled by an ISC rate (k_{ISC}) that dominates over fluorescence (k_{Fl}) and internal conversion (k_{IC}) rates ($k_{ISC} > k_{Fl} + k_{IC}$). These results establish a clear, generalizable blueprint for breaking the lifetime ceiling of pure organic p-TADF materials.

Persistent thermally activated delayed fluorescence (p-TADF) has recently emerged as a promising class of organic afterglow systems [1–4]. Unlike organic room-temperature phosphorescence (ORTP), which originates from the direct decay of triplet (T) excitons [5–10], p-TADF arises from the emission of singlet (S) excitons that are thermally repopulated via reverse intersystem crossing (rISC). This mechanism effectively lowers the required excitation energy by an amount approximately equal to the singlet-triplet energy gap (ΔE_{S1T1}), thereby enabling afterglow emission at lower excitation energies and/or shorter wavelengths [11–17]. Moreover, the thermally activated nature of p-TADF may help alleviate thermal quenching of T excitons at elevated temperatures [2, 18].

Nevertheless, p-TADF emitters typically exhibit considerably shorter lifetimes (τ) than their ORTP counterparts due to a fundamental kinetic trade-off. Achieving pure p-TADF demands that the rISC rate constant (k_{rISC}) greatly exceed the combined rates of phosphorescence (k_{Ph}) and non-radiative T_1 decay ($k_{nr,T}$), that is, $k_{rISC} \gg k_{Ph} + k_{nr,T}$. However, an excessively large k_{rISC} inevitably shortens the τ_{DF}, yielding $\tau_{DF} \ll \tau_{Ph}$. Given the scarcity of phosphorescent cores with ultra-long τ_{Ph}, most reported pure

Yue Lei and Ruyi Liu contributed equally to this work.

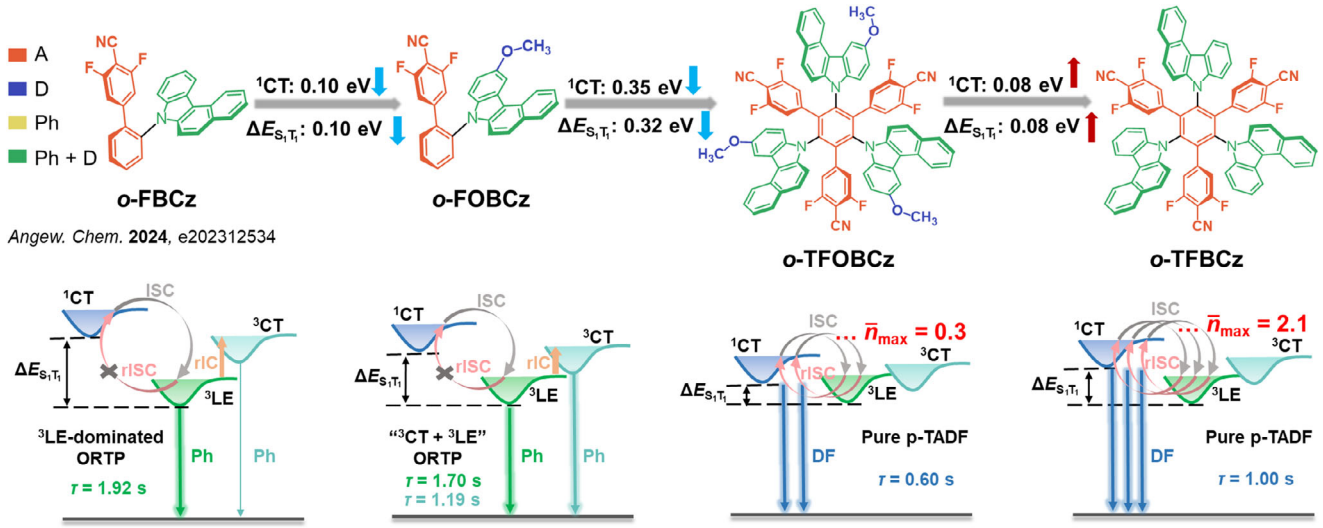

SCHEME 1 | Schematic illustration of the structural evolution across the four target compounds and their corresponding excited-state pathways.

p-TADF materials display τ_{DF} values below 0.6 s (Table S1) [11–17, 19–26]. This limitation underscores that optimizing k_{rISC} alone is insufficient for achieving extended τ_{DF} and highlights the necessity of comprehensive, multi-parameter design strategies.

To move beyond a sole focus on modulating k_{rISC}, we examined the potential of leveraging exciton cycling between S_1 and T_1 states. In principle, if each exciton undergoes multiple intersystem crossing (ISC)/rISC cycles prior to radiative decay, the effective τ_{DF} can be extended without necessitating a substantial suppression of k_{rISC}. Foundational evidence for this concept comes from Berberan-Santos and co-workers, who revealed extensive ISC/rISC cycling in the TADF of C_{70} and quantified an average cycle number ($\bar{n}$) of ~ 20 per exciton at room temperature [27]. More recently, analogous cycling behavior has been noted in perovskite-based p-TADF systems by Yan et al. [28] and explicitly proposed by Monkman and colleagues as a means to extend lifetimes in exciplex-based sub-microsecond TADF [29]. Inspired by these precedents, we hypothesized that intentionally engineering multiple ISC/rISC cycles in purely organic p-TADF fluorophores could offer a powerful route to prolonged τ_{DF}. To date, however, no dedicated molecular design strategy has been developed to implement this idea.

Herein we introduce a synergistic approach that simultaneously modulates k_{rISC} and promotes S_1–T_1 exciton cycling, thereby extending the effective τ_{DF} of pure p-TADF materials. The strategy rests on two complementary principles. First, k_{rISC} should be minimized while still satisfying the essential kinetic requirement for pure p-TADF ($k_{rISC} \gg k_{Ph} + k_{nr,T}$). This is achieved by employing a long-τ_{Ph} phosphorescent T_1 core and fine-tuning ΔE_{S1T1}. Second, to enable efficient exciton cycling, the forward ISC rate (k_{ISC}) must dominate over the combined rates of fluorescence (Fl) and internal conversion (IC) from S_1, that is, $k_{ISC} > k_{Fl} + k_{IC}$. Crucially, we realize this condition by suppressing k_{Fl} and k_{IC} rather than by inflating k_{ISC}, as enhancing k_{ISC} often inadvertently accelerates k_{rISC} [30], and thus counteracts lifetime extension.

Guided by these principles, we selected the *ortho*-linked donor–acceptor (D–A) scaffold *o*-FBCz (Scheme 1) as a molecular platform for this study [31]. Its charge-transfer (CT) S_1 state inherently possesses a very low k_{Fl} (1.79×10^7 s^{-1}; Table S2) and minimal k_{IC} (Figure S1), while the locally excited (LE) T_1 state, localized on the 7*H*-benzo[*c*]carbazole (BCz) subunit, exhibits a relatively long τ_{Ph} even in a moderately rigid matrix such as unannealed poly(methyl methacrylate) (PMMA) (1.92 s; Figure 1e). We therefore reasoned that targeted structural modification of *o*-FBCz—specifically, a modest reduction of ΔE_{S1T1} while preserving these favorable kinetic properties—would yield a pure p-TADF material capable of sustaining extended τ_{DF} through sustained S_1–T_1 exciton cycling.

To implement this strategy, we designed *o*-FOBCz by appending a methoxy substituent at the 10-position of the BCz moiety, yielding the OBCz subunit (Scheme 1). Density functional theory (DFT) calculations indicate that this -OMe group elevates the HOMO energy by ~0.09 eV while barely affecting the T_1 energy (Figure S2). Retaining the ^{1}CT and ^{3}LE characters of S_1 and T_1 states, respectively, this modification is predicted to narrow ΔE_{S1T1} relative to *o*-FBCz.

Consistent with this prediction, the ^{1}CT-dominated S_1 state of *o*-FOBCz lies lower in energy than that of *o*-FBCz, whereas the T_1 state preserves its ^{3}LE character and energy (Figure 1a–c, Figures S3–S5). In toluene solution, *o*-FOBCz maintains a comparably low k_{Fl} (1.56×10^7 s^{-1}; Table S2), verifying retention of the desirable S_1-state kinetics. When doped into PMMA at 1 wt%, the resulting *o*-FOBCz@PMMA film exhibits a green afterglow lasting over 10 s (Figure 1f and Movie S1). However, its delayed photoluminescence (PL) spectrum comprises two distinct emission bands (Figure 1c): a dominant lower-energy ^{3}LE phosphorescence band from T_1, and a weaker higher-energy band assigned to ^{3}CT phosphorescence from T_2 (rather than p-TADF), given its noticeably red-shift relative to the prompt fluorescence (PF) [32, 33]. Accordingly, *o*-FOBCz@PMMA operates as a hybrid ^{3}LE/^{3}CT ORTP material, with corresponding τ_{Ph} of 1.70 and 1.19 s, respectively (Figure 1e).

Thus, although replacing BCz with OBCz reduces ΔE_{S1T1} by 0.10 eV in PMMA, it activates an undesired $T_1 \rightarrow T_2$ reverse

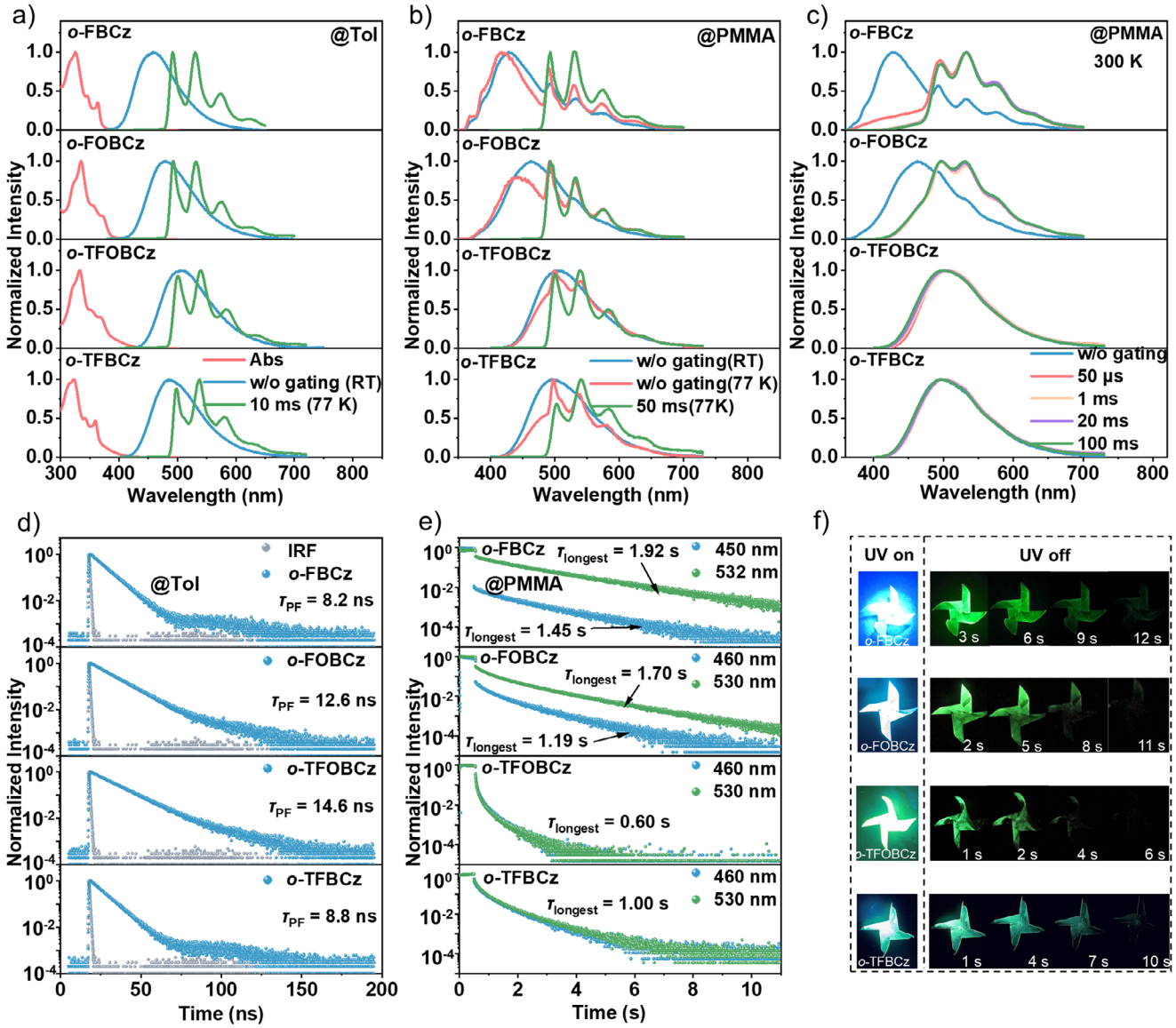

FIGURE 1 | Comparative photophysical characterization of *o*-FBCz, *o*-FOBCz, *o*-TFOBCz, and *o*-TFBCz in solution (toluene) and solid state (PMMA matrix). (a) UV-Vis absorption, steady-state PL (300 K), and time-gated PL (77 K, 10 ms) spectra in toluene. (b) Steady-state (77 and 300 K) and time-gated (77 K, 50 ms) PL spectra in PMMA. (c) Steady-state and time-resolved PL spectra in PMMA at 300 K (*o*-FBCz and *o*-FOBCz: λ_{ex} = 320 nm, *o*-TFOBCz and *o*-TFBCz: λ_{ex} = 370 nm). (d, e) PL decay profiles in toluene and PMMA at 300 K (λ_{ex} = 320 nm); (f) Photographs showing the afterglow emission of the PMMA-doped films at 300 K (λ_{ex} = 355 nm, excitation pulse width: 0.5 s).

internal conversion (rIC) channel over the targeted $T_1 \rightarrow S_1$ rISC pathway. To achieve a p-TADF-type afterglow, a further reduction of ΔE_{S1T1} is required. We therefore elaborated the single D–A motif of *o*-FOBCz into a triple D–A architecture, yielding *o*-TFOBCz (Scheme 1). This design leverages the established ability of multiple D–A units to stabilize the CT-charactered S_1 state [34].

As shown in Figure 1b, o-TFOBCz features a stabilized ^{1}CT-type S_1 state relative to *o*-FOBCz, while the T_1 energy remains essentially unchanged, resulting in a contracted ΔE_{S1T1} of 0.32 eV in PMMA. Notably, *o*-TFOBCz also ratains an exceptionally low k_{FI} (7.14×10^6 s^{-1}; Table 1), a key feature for promoting sustained ISC/rISC cycling. At 300 K, *o*-TFOBCz@PMMA produces a green afterglow lasting 5 s under either 365 or 405 nm excitation (Figure 1f, Movies S2, S3).

Temperature-dependent PL measurements reveal progressive activation of TADF with increasing temperature (Figure 2a–c, Figures S7, S8). At 80–100 K, the delayed PL spectrum consists exclusively of ^{3}LE phosphorescence. A ^{3}CT band emerges by 120 K, and by 180 K, three components, namely the TADF (^{1}CT) band, ^{3}CT band, and ^{3}LE band, are required to adequately fit the spectrum. Above 280 K, solely the TADF band persists. This assignment is supported by its spectral overlap with the steady-state PL (Figure 1c) and by identical decay kinetics recorded at 460 nm (free of T_1-phosphorescence) and 530 nm (dominated by T_1-phosphorescence) (Figure 1e).

Notably, the longest lifetime component ($\tau_{longest}$) of *o*-TFOBCz@PMMA reaches 0.60 s at 300 K, placing it among the longest-lived pure ambient p-TADF systems reported without

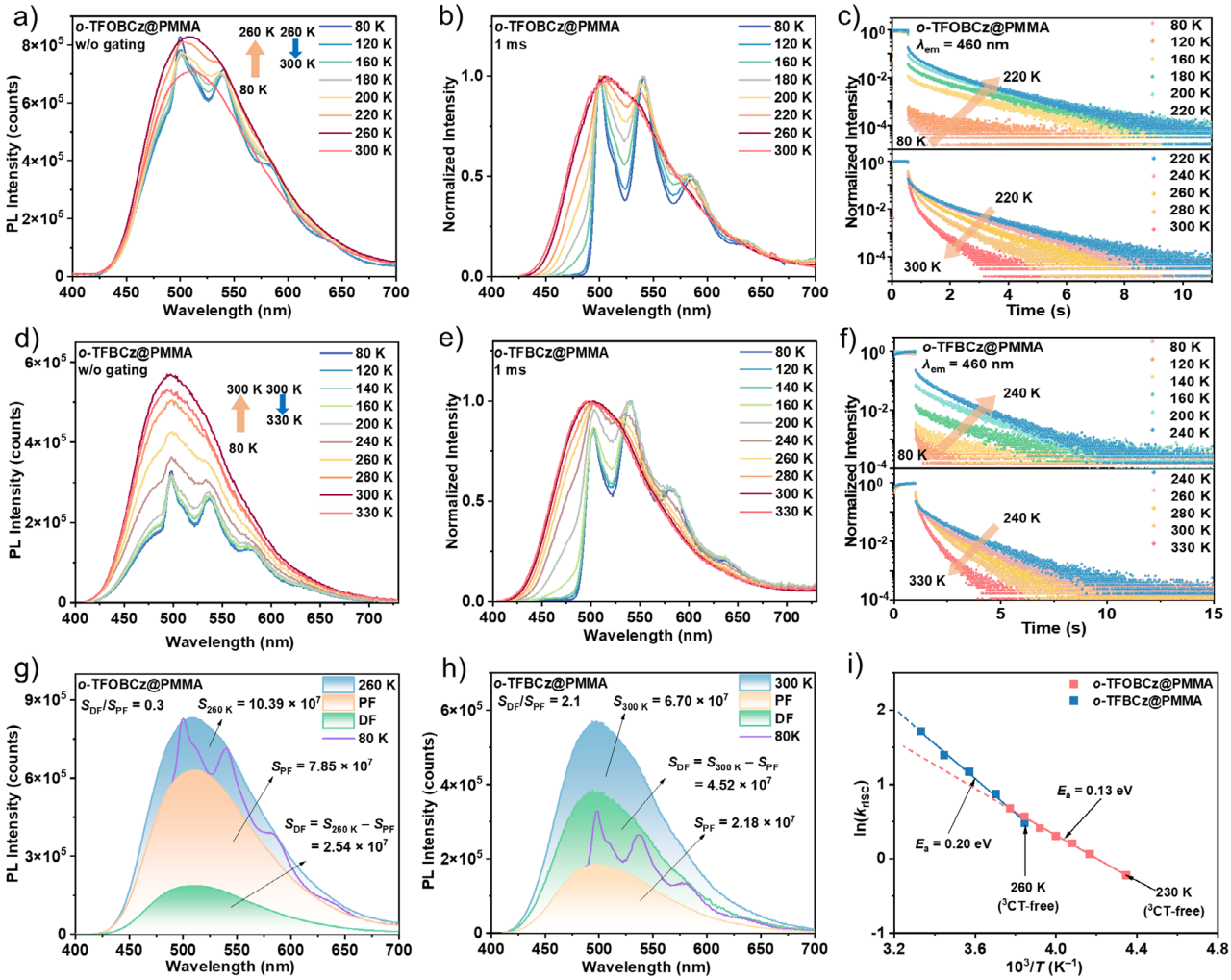

FIGURE 2 | Temperature-dependent PL characterization of *o*-TFOBCz@PMMA and *o*-TFBCz@PMMA. (a, d) Steady-state PL spectra (λ_{ex} = 370 nm). (b, e) Normalized 1 ms delayed PL spectra (λ_{ex} = 370 nm). (c, f) PL decay kinetics monitored at 460 nm (*o*-TFOBCz@PMMA: λ_{ex} = 355 nm, excitation pulse width: 0.5 s; *o*-TFBCz@PMMA: λ_{ex} = 370 nm, excitation pulse width: 1.0 s). (g, h) Estimated $\bar{n}_{max}$. (i) Arrhenius plot of the k_{rISC} versus reciprocal temperature.

post-annealing treatment. Moreover, this material already exhibits pure TADF-type afterglow at 280 K, with an even longer $\tau_{longest}$ of 0.77 s (Figure S9, Table S3). The observed decline in steady-state PL intensity from 280 to 300 K (Figure S7) further suggests that a slight enlargement of ΔE_{S1T1} might prolong the afterglow lifetime even further.

Building on the findings that *o*-FBCz possesses a larger ΔE_{S1T1} than *o*-FOBCz, we synthesized *o*-TFBCz by excising the methoxy substituents from *o*-TFOBCz (Scheme 1). As shown in Figure 1a–c, this modification raises the S_1 energy by ~0.08 eV while leaving the T_1 energy essentially unchanged, thereby widening ΔE_{S1T1} by a corresponding margin (Table 1). At 300 K, *o*-TFBCz@PMMA exhibits a bluish-green afterglow lasting 10 s under either 365 or 405 nm excitation (Figure 1f, Figure S10, Movies S4–S5), with an afterglow spectral maximum of 494 nm, confirming a low excitation-energy requirement characteristic of p-TADF materials.

Crucially, its delayed PL spectrum at 300 K coincides with the steady-state spectrum and exhibits wavelength-independent decay kinetics (Figure 1c,e), validating its pure p-TADF character. The onset temperatures for both the ^{3}CT and TADF emission bands are ~20 K higher than those observed for *o*-TFOBCz@PMMA (Figures S11, S12), indicative of elevated energy barriers for the thermally activated process. Impressively, the $\tau_{longest}$ of *o*-TFBCz@PMMA reaches 1.00 s at 300 K, establishing a new benchmark for ambient pure p-TADF systems. Since both *o*-TFOBCz@PMMA and *o*-TFBCz@PMMA exhibit comparable τ_{Ph} at 80 K (~2.5 s; Figure S13), their k_{Ph} and $k_{nr,T}$ from the T_1 state are expected to be similar. The extended τ_{DF} of *o*-TFBCz@PMMA thus can be attributed, at least in part, to a slower rISC process. Gratifyingly, τ_{DF} retains as long as 0.64 s even at 330 K (Figure 2f and Figure S14, Table S5), underscoring its potential for high-temperature applications (Figure S16).

These observations gain clearer context when compared with the single-D-A analog *o*-FBCz, which shares the same BCz-localized ^{3}LE T_1 state. While *o*-FBCz@PMMA exhibits ^{3}LE-dominated phosphorescence under ambient conditions (τ_{Ph} = 1.92 s; Figure 1e), o-TFBCz@PMMA achieves a τ_{DF} as long as 1.00 s. This discrepancy challenges the conventional single-cycle ISC/rISC model, which requires $k_{rISC} \gg k_{Ph} + k_{nr,T}$, a condition inconsistent with the observed lifetimes. The multiexponential

TABLE 1 | Summary of photophysical properties of *o*-TFOBCz and *o*-TFBCz.

Compd.	λ_{Fl} [nm]	λ_{Ph} [nm]	ΔE_{S1T1} [eV][a]	τ_{PF} [ns]	τ_{DF} [s][c]	φ_{DF}[c]	φ_{PF}	φ_{ISC}[b]	φ_{IC}[b]	k_{Fl} [s^{-1}][b]	k_{ISC} [s^{-1}][b]	k_{IC} [s^{-1}][b]
o-TFOBCz	506[b]/503[c]	540[b]/538[c]	0.24[b]/0.25[c]	14.6[b]/22.6[c]	0.60[c]	4.2%[c]	10.4%[b]/29.3%[c]	47.4%[b]	42.1%[b]	7.14×10^6	32.6×10^6	29.0×10^6
o-TFBCz	489[b]/494[c]	539[b]/540[c]	0.31[b]/0.33[c]	8.8[b]/14.0[c]	1.00[c]	20.3%[c]	6.0%[b]/9.8%[c]	76.0%[b]	17.9%[b]	6.86×10^6	86.4×10^6	20.4×10^6

[a]Estimated from the onset of the corresponding PL spectrum.
[b]Measured in toluene.
[c]Measured in PMMA.

decay kinetics of *o*-TFBCz@PMMA at 300 K, in contrast to the near single-exponential decay of *o*-FBCz@PMMA (Figure 1e), provides compelling evidence for the occurrence of multiple ISC/rISC cycles (Figure S15 and accompanying discussion).

Direct evidence for multiple ISC/rISC cycles emerges from temperature-dependent steady-state PL measurements. The PL intensity of *o*-TFBCz@PMMA increases substantially between 160 and 300 K, reflecting a growing TADF contribution to the total emission (Figure 2d). Spectral deconvolution, assuming invariant PF quantum yield (φ_{PF}) and absorbance [35], yields a $\varphi_{DF}/\varphi_{PF}$ ratio of 2.1 at 300 K (Figure 2h). This ratio corresponds to the average number of ISC/rISC cycles per exciton ($\bar{n}$) [27]. With a total PL quantum yield ($\varphi_{PF} + \varphi_{DF}$) of 30.1%, φ_{DF} is calculated to be 20.3% at 300 K and remains robust at elevated temperatures: 18.6% at 320 K and 18.4% at 330 K (Figure S11). These metrics establish *o*-TFBCz as one of the premier pure ambient p-TADF emitters reported to date.

In contrast, the maximum average cycle number ($\bar{n}_{max}$) for *o*-TFOBCz@PMMA reaches only 0.3. To pinpoint the origin of this marked difference in ISC/rISC cycling efficiency, ISC efficiencies (φ_{ISC}) of both emitters were quantified in toluene (Figures S17–S18). Using φ_{ISC} together with fluorescence efficiency (φ_{Fl}) and lifetime (τ_{Fl}) data, we determined the rate constants k_{Fl}, k_{ISC} and k_{IC}. As summarized in Table 1, o-TFBCz exhibits a k_{Fl} comparable to that of *o*-TFOBCz (6.86×10^6 vs. 7.14×10^6 s^{-1}), yet a substantially higher k_{ISC} (8.64×10^7 vs. 3.26×10^7 s^{-1}) and a lower k_{IC} (2.04×10^7 vs. 2.90×10^7 s^{-1}). These kinetic advantages strongly promote exciton cycling from S_1 to T_1 state, yielding the significantly larger $\bar{n}_{max}$ observed.

Arrhenius plots of k_{rISC} versus reciprocal temperature (Figure 2i) indicate nearly identical k_{rISC} values for the two films at 270 K. At this temperature, however, the $\tau_{longest}$ of *o*-TFBCz@PMMA obviously exceeds that of *o*-TFOBCz@PMMA (1.16 vs. 0.82 s), accompanied by a markedly higher normalized pre-exponential factor (25% vs. 7%). These findings collectively indicate that the superior afterglow performance of *o*-TFBCz@PMMA arises from its enhanced ISC/rISC cycling efficiency.

The derived activation energies (E_a) are 0.20 eV for *o*-TFBCz@PMMA and 0.13 eV for *o*-TFOBCz@PMMA. The near-equivalence of the difference in E_a (ΔE_a) and the difference in ΔE_{S1T1} ($\Delta\Delta E_{S1T1}$) suggests that the thermally activated process likely involves direct participation of the S_1 and T_1 states. The small offsets between the spectroscopically determined ΔE_{S1T1} (estimated from the onsets of the corresponding fluorescence and phosphorescence spectra) and the measured E_a values (0.33 vs. 0.20 eV for *o*-TFBCz@PMMA; 0.25 vs. 0.13 eV for *o*-TFOBCz@PMMA) can be reasonably attributed to uncertainty in determining the S_1 onset energy due to the slow rise of the fluorescence spectrum [36].

In summary, this work demonstrates a synergistic design strategy that couples precise modulation of k_{rISC} with deliberate promotion of ISC/rISC cycling to achieve prolonged τ_{DF} in pure p-TADF systems. Side-by-side comparison of the triple D–A emitters *o*-TFBCz and *o*-TFOBCz reveals that a larger ΔE_{S1T1} effectively suppresses k_{rISC}, while an elevated k_{ISC} enhances ISC/rISC cycling efficiency, collectively contributing to the marked extension of

τ_{DF}. Strikingly, *o*-TFBCz@PMMA attains ambient pure p-TADF with a τ_{DF} up to 1.00 s, despite originating from a phosphorescence core with a τ_{Ph} of only 1.92 s, underscoring the profound impact of multi-cycle exciton dynamics. These results suggest that employing phosphorescent cores with intrinsically longer τ_{Ph} could further extend τ_{DF}. Moreover, the material exhibits a bluish-green afterglow under blue-light excitation, and the system exhibits outstanding thermal stability, placing it among the highest-performance p-TADF materials reported to date.

Therefore, these findings establish a clear and actionable set of design principles for developing high-performance pure p-TADF materials. To construct an ideal p-TADF emitter, the following features are propitious for prolonging the afterglow lifetime: a phosphorescence core with a long room-temperature τ_{Ph}, a moderate ΔE_{S1T1} that yields a relatively small k_{rISC} (provided that $k_{rISC} \gg k_{Ph} + k_{nr,T}$), and a large φ_{ISC} to promote efficient ISC/rISC multiple cycling. Meanwhile, a high φ_{ISC}, along with low φ_{IC} and $\varphi_{nr,T}$, is beneficial for increasing the afterglow quantum efficiency. In this study, the effective π–π interactions between the D and A subunits are responsible for suppressing the IC process, resulting in a high φ_{ISC} in the objective triple-D–A-featured fluorophores.

Author Contributions

Yue Lei: conceptualization, validation, writing – original draft, investigation, methodology, visualization, software, formal analysis. **Ruyi Liu**: validation, investigation, software, formal analysis, conceptualization, visualization. **Yuling He**: visualization, validation. **Guiyin Luo**: visualization, validation. **Chuanhao Liu**: validation, visualization. **Jiaqi Su**: validation, visualization. **Binhao Li**: validation, visualization. **Xue Long**: validation, visualization. **Yuchang Tan**: validation, visualization. **Yanju Luo**: validation, visualization. **Hailin Qiu**: validation, visualization. **Yan Huang**: writing – review and editing, resources, project administration, supervision. **Zhiyun Lu**: conceptualization, writing – review and editing, funding acquisition, supervision, project administration, data curation, resources, methodology.

Acknowledgments

The authors acknowledge the financial support from the National Natural Science Foundation of China (No. 22475138) and Fundamental Research Funds for the Central Universities. We thank Dr. Y. Wang of the Analytical & Testing Center, Sichuan University, for photophysical measurements and Dr. M. Yang of the Comprehensive Training Platform of Specialized Laboratory, College of Chemistry, Sichuan University, for help in crystallographic characterizations.

Conflicts of Interest

The authors declare no conflicts of interest.

Data Availability Statement

The data that support the findings of this study are available on request from the corresponding author. The data are not publicly available due to privacy or ethical restrictions.

References

1. Y. Chen, J. Lei, P. Liu, et al., "Unveiling the Evolution of Afterglow in Diboraanthracene Scaffolds: From Thermally Activated Delayed Fluorescence to Room-Temperature Phosphorescence," *Journal of the American Chemical Society* 147 (2025): 45603–45617, https://doi.org/10.1021/jacs.5c16948.

2. J. Jovaišaitė, S. Kirschner, S. Raišys, et al., "Diboraanthracene-Doped Polymer Systems for Colour-Tuneable Room-Temperature Organic Afterglow," *Angewandte Chemie International Edition* 62 (2023): e202215071.

3. J. Wang, Y. Yang, K. Li, L. Zhang, and Z. Li, "Purely Organic Fluorescence Afterglow: Visible-Light-Excitation, Inherent Mechanism, Tunable Color, and Practical Applications With Very Low Cost," *Angewandte Chemie International Edition* 62 (2023): e202304020, https://doi.org/10.1002/anie.202304020.

4. X. Wang, Y. Sun, G. Wang, J. Li, X. Li, and K. Zhang, "TADF-Type Organic Afterglow," *Angewandte Chemie International Edition* 60 (2021): 17138–17147, https://doi.org/10.1002/anie.202105628.

5. X. Shen, Y. Luo, K. Chen, et al., "A Red Ambient Afterglow Material With Lifetime of 0.5 s and Efficiency Over 12%," *Chemical Communications* 59 (2023): 7036–7039, https://doi.org/10.1039/D3CC01910A.

6. K. Wang, C. Liu, Y. He, et al., "NPA6: A Molecule for Non-Covalently Linked Radical-Enhanced ISC and High-Performance Photopolymerization With Afterglow," *Angewandte Chemie International Edition* 64 (2025): e202509520, https://doi.org/10.1002/anie.202509520.

7. H. Zheng, P. Cao, Y. Wang, X. Lu, and P. Wu, "Ultralong Room-Temperature Phosphorescence From Boric Acid," *Angewandte Chemie International Edition* 60 (2021): 9500–9506, https://doi.org/10.1002/anie.202101923.

8. H. Zheng, Y. Wang, P. Cao, and P. Wu, "Color-Tunable Ultralong Room Temperature Phosphorescence From EDTA," *Chemical Communications* 57 (2021): 3575–3578, https://doi.org/10.1039/D1CC00207D.

9. J. Song, Y. Wang, L. Qu, et al., "Room-Temperature Phosphorescence of Pure Axially Chiral Bicarbazoles," *Journal of Physical Chemistry Letters* 13 (2022): 5838–5844, https://doi.org/10.1021/acs.jpclett.2c01614.

10. B. Wang, X. Yuan, X. Lv, et al., "Carbon Dots-Based Room-Temperature Phosphorescent Test Strip: Visual and Convenient Water Detection in Organic Solvents," *Dyes and Pigments* 189 (2021): 109226, https://doi.org/10.1016/j.dyepig.2021.109226.

11. X. Zou, N. Gan, Z. Lin, et al., "Short-Range Charge Transfer for Efficient Ultra-Narrowband Deep Blue Afterglow," *Nature Communications* 16 (2025): 6412, https://doi.org/10.1038/s41467-025-61513-7.

12. X. Li, G. Wang, Z. Ye, B. Xu, H. Gao, and K. Zhang, "Highly-Efficient Visible-Light-Excitable TADF-Type Organic Afterglow Materials via Intramolecular Charge Transfer Technology," *Advanced Optical Materials* 13 (2025): 2403551, https://doi.org/10.1002/adom.202403551.

13. J. Zhang, W. Zhou, L. Yang, et al., "Visible-Light Excitable Thermally Activated Delayed Fluorescence From Hydrogen-Bonded D-A Aromatic N-Heterocycle/Polymer Material and the Application for Anti-Counterfeiting," *Dyes and Pigments* 223 (2024): 111927, https://doi.org/10.1016/j.dyepig.2023.111927.

14. G. Wang, S. Ding, J. Li, et al., "A Narrow-Band Deep-Blue MRTADF-Type Organic Afterglow Emitter," *Chemical Communications* 59 (2023): 12302–12305, https://doi.org/10.1039/D3CC04012G.

15. X. Chen, G. Wang, X. Piao, and K. Zhang, "Achieving Visible-Light-Excitable Blue TADF-Type Afterglow via Delicate Control of Excited States in Difluoroboron β-Diketonate Systems," *Chemistry—A European Journal* 30 (2024): e202303834, https://doi.org/10.1002/chem.202303834.

16. S. Shen, Y. Sun, D. Wang, Z. Zhang, Y. Shi, and Z. Wang, "Efficient Blue TADF-Type Organic Afterglow Material via Boric Acid-Assisted Confinement," *Chemical Communications* 58 (2022): 11418–11421, https://doi.org/10.1039/D2CC04544C.

17. W. Xia, J. Li, G. Wang, et al., "Visible-Light-Excitable Sky-Blue TADF-Type Organic Afterglow," *Journal of Physical Chemistry C* 127 (2023): 19805–19813, https://doi.org/10.1021/acs.jpcc.3c04948.

18. Y. Yang, Y. Liang, Y. Zheng, et al., "Efficient and Color-Tunable Dual-Mode Afterglow From Large-Area and Flexible Polymer-Based Transparent Films for Anti-Counterfeiting and Information Encryption,"

Angewandte Chemie International Edition 61 (2022): e202201820, https://doi.org/10.1002/anie.202201820.

19. K. Chen, Y. Jiang, Y. Zhu, et al., "Host to Regulate the T_1 –S_1 and T_1 –S_0 Processes of Guest Excitons in Doped Systems to Control the TADF and RTP Emissions," *Journal of Materials Chemistry C* 10 (2022): 11607–11613, https://doi.org/10.1039/D2TC02167F.

20. G. Wang, J. Li, X. Li, et al., "Two-Component Design Strategy: TADF-Type Organic Afterglow for Time-Gated Chemodosimeters," *Chemical Engineering Journal* 431 (2022): 134197, https://doi.org/10.1016/j.cej.2021.134197.

21. X. Deng, J. Huang, J. Li, G. Wang, and K. Zhang, "Sonication-Responsive Organic Afterglow Emulsions," *Advanced Functional Materials* 33 (2023): 221496, https://doi.org/10.1002/adfm.202214960.

22. Z. Mo, G. Wang, J. Li, Q. Yan, and K. Zhang, "Dopant-Matrix Afterglow Systems: Manipulation of Room-Temperature Phosphorescence/Thermally Activated Delayed Fluorescence Afterglow Mechanism via Mismatch/Match of Intermolecular Charge Transfer Between Dopants and Matrices," *Journal of Physical Chemistry Letters* 14 (2023): 11142–11151, https://doi.org/10.1021/acs.jpclett.3c03060.

23. X. Wang, J. Li, Y. Zeng, et al., "Merging Thermally Activated Delayed Fluorescence and Two-Photon Ionization Mechanisms for Highly Efficient and Ultralong-Lived Organic Afterglow," *Chemical Engineering Journal* 460 (2023): 141916, https://doi.org/10.1016/j.cej.2023.141916.

24. M. Wu, J. Li, J. Huang, et al., "The Unexpected Mechanism of Transformation From Conventional Room-Temperature Phosphorescence to TADF-Type Organic Afterglow Triggered by Simple Chemical Modification," *Journal of Materials Chemistry C* 11 (2023): 2291–2301, https://doi.org/10.1039/D2TC05261J.

25. G. Wang, S. Ding, J. Li, et al., "Intrinsic Narrowband Organic Afterglow," *Chemistry of Materials* 36 (2024): 3000–3012, https://doi.org/10.1021/acs.chemmater.4c00161.

26. J. Zhang, J. Li, X. Li, et al., "Boosting Organic Afterglow Efficiency via Triplet–Triplet Annihilation and Thermally-activated Delayed Fluorescence," *Journal of Materials Chemistry C* 10 (2022): 4795–4804, https://doi.org/10.1039/D1TC04903H.

27. C. Baleizão and M. N. Berberan-Santos, "Thermally Activated Delayed Fluorescence as a Cycling Process Between Excited Singlet and Triplet States: Application to the Fullerenes," *Journal of Chemical Physics* 126 (2007): 204510, https://doi.org/10.1063/1.2734974.

28. B. Zhou and D. Yan, "Simultaneous Long-Persistent Blue Luminescence and High Quantum Yield Within 2D Organic–Metal Halide Perovskite Micro/Nanosheets," *Angewandte Chemie International Edition* 58 (2019): 15128–15135, https://doi.org/10.1002/anie.201909760.

29. D. Graves, V. Jankus, F. B. Dias, and A. Monkman, "Photophysical Investigation of the Thermally Activated Delayed Emission From Films of M-MTDATA:PBD Exciplex," *Advanced Functional Materials* 24 (2013): 2343–2351, https://doi.org/10.1002/adfm.201303389.

30. K. Goushi, K. Yoshida, K. Sato, and C. Adachi, "Organic Light-Emitting Diodes Employing Efficient Reverse Intersystem Crossing for Triplet-to-Singlet State Conversion," *Nature Photonics* 6 (2012): 253–258, https://doi.org/10.1038/nphoton.2012.31.

31. R. Liu, C. Liu, C. Fu, et al., "Ambient Phosphor With High Efficiency and Long Lifetime in Poly(Methyl Methacrylate) Through Charge-Transfer-Mediated Triplet Exciton Formation for Photolithography Applications," *Angewandte Chemie International Edition* 63 (2024): e202312534, https://doi.org/10.1002/anie.202312534.

32. K. Chen, Y. Luo, M. Sun, et al., "Acquiring Charge-Transfer-Featured Single-Molecule Ultralong Organic Room Temperature Phosphorescence via Through-Space Electronic Coupling," *Angewandte Chemie International Edition* 63 (2024): e202314447, https://doi.org/10.1002/anie.202314447.

33. K. Chen, B. Li, C. Liu, et al., "Achieving Charge-Transfer-Featured Organic Room-Temperature Phosphorescence With Combined High Efficiency and Long Lifetime via V-Shaped D–A Dyads," *Angewandte Chemie International Edition* 64 (2025): e202508776, https://doi.org/10.1002/anie.202508776.

34. X. Zheng, R. Huang, C. Zhong, et al., "Achieving 21% External Quantum Efficiency for Nondoped Solution-Processed Sky-Blue Thermally Activated Delayed Fluorescence OLEDs by Means of Multi-(Donor/Acceptor) Emitter With Through-Space/-Bond Charge Transfer," *Advanced Science* 7 (2020): 1902087, https://doi.org/10.1002/advs.201902087.

35. I. S. Park, K. Matsuo, N. Aizawa, and T. Yasuda, "High-Performance Dibenzoheteraborin-Based Thermally Activated Delayed Fluorescence Emitters: Molecular Architectonics for Concurrently Achieving Narrowband Emission and Efficient Triplet–Singlet Spin Conversion," *Advanced Functional Materials* 28 (2018): 1802031, https://doi.org/10.1002/adfm.201802031.

36. F. B. Dias, "Kinetics of Thermal-Assisted Delayed Fluorescence in Blue Organic Emitters With Large Singlet–Triplet Energy Gap," *Philosophical Transactions of the Royal Society A: Mathematical, Physical and Engineering Sciences* 373 (2015): 20140447, https://doi.org/10.1098/rsta.2014.0447.

Supporting Information

Additional supporting information can be found online in the Supporting Information section.

Supporting File 1: anie73257-sup-0001-SuppMat.docx.
Supporting File 2: anie73257-sup-0002-MovieS1.mp4.
Supporting File 3: anie73257-sup-0003-MovieS2.mp4.
Supporting File 4: anie73257-sup-0004-MovieS3.mp4.
Supporting File 5: anie73257-sup-0005-MovieS4.mp4.
Supporting File 6: anie73257-sup-0006-MovieS5.mp4.
Supporting File 7: anie73257-sup-0007-MovieS6.mp4.
Supporting File 8: anie73257-sup-0008-MovieS7.mp4.
Supporting File 9: anie73257-sup-0009-MovieS8.mp4.
Supporting File 10: anie73257-sup-0010-MovieS9.mp4.
Supporting File 11: anie73257-sup-0011-MovieS10.mp4.
Supporting File 12: anie73257-sup-0012-MovieS11.mp4.
Supporting File 13: anie73257-sup-0013-Data.zip.